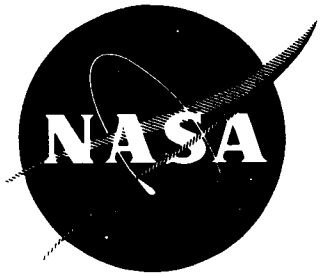

NASA CR-54768

F U E L C E L L R E S E A R C H

AN INVESTIGATION OF NON-STEADY-STATE OPERATION

by

T. J. Gray, A. A. Schneider, R. B. Rozelle and M. L. Soeder

prepared for

NATIONAL AERONAUTICS AND SPACE ADMINISTRATION

GRANT NsG-384

Alfred University
Alfred, New York

NOTICE

This report was prepared as an account of Government sponsored work. Neither the United States, nor the National Aeronautics and Space Administration (NASA), nor any person acting on behalf of NASA:

A.) Makes any warranty or representation, expressed or implied, with respect to the accuracy, completeness, or usefulness of the information contained in this report, or that the use of any information, apparatus, method, or process disclosed in this report may not infringe privately owned rights; or

B.) Assumes any liabilities with respect to the use of, or for damages resulting from, the use of any information, apparatus, method, or process disclosed in this report.

As used above, "person acting on behalf of NASA" includes any employee or contractor of NASA, or employee of such contractor, to the extent that such employee or contractor of NASA, or employee of such contractor prepares, disseminates, or provides access to, any information pursuant to his employment or contract with NASA, or his employment with such contractor.

Requests for copies of this report should be referred to

National Aeronautics and Space Administration
Office of Scientific and Technical Information
Attention: AFSS-A
Washington, D. C. 20546

FINAL REPORT

FUEL CELL RESEARCH

An Investigation of Non-Steady-State Operation

by

T. J. Gray, A. A. Schneider, R. B. Rozelle, M. L. Soeder

prepared for

NATIONAL AERONAUTICS AND SPACE ADMINISTRATION

Period: June 1, 1963 - June 1, 1965

Grant NsG-384

Technical Management
NASA Lewis Research Center
Cleveland, Ohio
Solar and Chemical Power Branch
Meyer R. Unger

ALFRED UNIVERSITY
Alfred, New York

December 1965

TABLE OF CONTENTS

PART I

PART II

LIST OF FIGURES

PART I

INTRODUCTION

This report is divided into three sections. The first is concerned with the investigation of the effect of pulsed loading on fuel cell operation. In this section is discussed the development of a working pulse loading device and the preliminary performance data of a fuel cell subjected to pulse loading. It was anticipated and later experimentally verified that pulsed loading would effect improvement in cell performance only if the average pulsed current were such that if the cell were operated at this current under steady load, concentration polarization would be the limiting factor in cell performance. Average pulsed current is defined as (current during fraction of cycle in which cell is loaded) x (fraction of cycle in which cell is loaded). For example, in order to realize an average current of 5 amp at 12% duty cycle, the current during the fraction of the cycle in which the cell is loaded must be 41.5 amp since 41.5 amp x 0.12 = 5 amp.

It must be realized, too, that a significant improvement in performance will be seen only if the IR drop due to the internal resistance of the cell is not too great. It might be said that, in general, improvement will be noted only if the knee of the potential-current curve under steady load occurs above 0.6 volt.

Inherent in the pulse loading system employed is a heavy anodic pulse of very short duration which occurs at the end of each duty cycle. This results in a secondary beneficial effect; investigation by Union Carbide Corporation (NASA Contract NAS3-6460) has demonstrated that a significant improvement in fuel cell operation can be achieved by heavy intermittent pulsing of a fuel cell, apparently resulting from catalyst activation.

The second portion of this report is a paper delivered in Brussels, Belgium, in June 1965, at a conference entitled "Journees International D'Etude des Piles Combustible". This paper is a compilation of the work done in this laboratory on the application of galvanostatic techniques to fuel cell electrode study; the title of the paper is "Application of Galvanostatic Studies to Fuel Cell Electrodes".

The third section is a Master's thesis by M. L. Soeder on the investigation by means of galvanostatic charging curves of the occlusion of hydrogen and of surface oxide formation in a series of palladium-gold alloys.

PULSE LOADING

EXPERIMENTAL

In order to investigate fuel cell performance under pulsed load, it was necessary first to develop a device suitable for switching the large currents developed by a fuel cell. Mechanical switches were eliminated because of their many limitations. These cannot be operated at frequencies much above 100 c/s and are not dependable because of contact bounce and contact burning at high currents. The silicon controlled rectifier, however, showed great promise and many circuits were designed which employed SCR's as the switching element. At least ten of the circuits designed failed due to one or both of the following reasons. Either there was not sufficient voltage available from the output of the inverter to turn off the SCR once it had reached the conduction state or, in the case where a transformer was added to give sufficient voltage the transformer saturated, created a large impedance in the load circuit, distorted the wave form and made it impossible to operate at high frequencies.

The latest circuit developed employs a transformer operating under non-saturating conditions. The circuit diagram is given in Figure 1. SCR_1 is fired by means of a pulse transformer at time t_1. The current surge through the primary of the transformer creates a large voltage across the secondary which charges capacitor C_1 through D_1. The diode prevents the capacitor from discharging after it has charged to its peaks voltage. At time t_2, SCR_2 is fired applying the capacitor voltage across SCR_1. This reverse bias turns off SCR_1 and when C_1 has discharged, SCR_2 turns off automatically.

This circuit, however, operates satisfactorily over only a very narrow range of frequencies and loads probably due to poor design in the transformer. New transformers are now being tested since these are fundamental to the inverter circuit.

In order to make a more versatile unit necessary for fundamental cell studies, a power supply was substituted for the transformer and C_1 was replaced with a variable capacitance. This auxiliary power supply produced the parasitic power which would otherwise be derived from the output of the inverter transformer. The result of this change is shown in the circuit diagram given in Figure 2. In this system, both SCR_1 and SCR_3 are fired at t_1, thus loading the fuel cell and charging C_2. SCR_3 turns off automatically when C_2 reaches peak voltage. As before, SCR_2 is fired at time t_2 applying the voltage across C_2 to SCR_1 thus effecting turnoff of SCR_1. SCR_2 turns off automatically when C_2 is discharged.

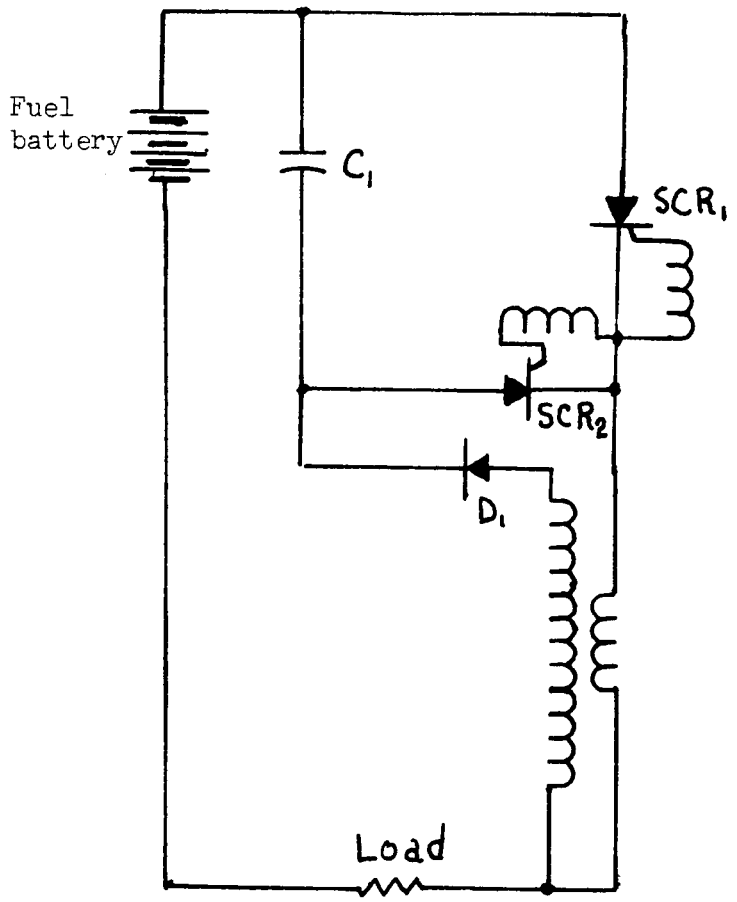

Figure 1. Circuit diagram of pulse loading system.

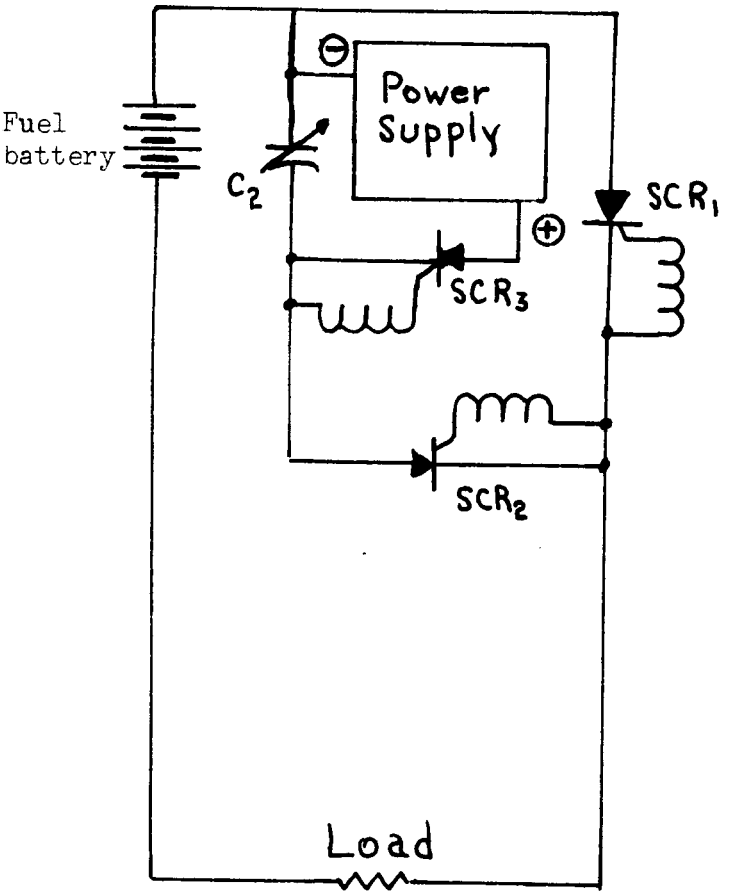

Figure 2. Circuit diagram of pulse loading system used for actual measurement.

A Parabam* pulse generator supplied the turn on pulse for the SCR's and also determines frequency and duty cycle.

The hydrogen-oxygen fuel cell studies employed a 30% potassium hydroxide electrolyte held in a 1/16-inch asbestos matrix. Both the potassium hydroxide and the asbestos were "carbonate free". The electrode material (Clevite nickel No. 3), obtained from Clevite Corporation, consisted of a nickel wire mesh covered with porous sintered nickel. This material was subjected to ultrasonic agitation in a 2% platinum-2% palladium chloride solution; a solution of the same composition was then employed to electrolytically co-deposit the platinum-palladium black as the catalyst. The electrodes, each of geometric area 3 in^2, were placed in a holder made of machined nickel sheet. The holder was designed so that the gases passed across the back of each electrode via a honeycomb of gas channels. The hydrogen and oxygen pressures were both 10 psi and the cells were operated at room temperature.

To measure the average potential of the cell under pulsed load, a Varian 10 millivolt recorder was connected across the cell by means of a potential divider. Since the response time of the recorder was much greater than the time of one cycle, an average potential was registered on the chart paper.

To be certain that this was the true average potential, oscilloscope photographs were taken of the cell potential when the cell had reached equilibrium under pulsed loading conditions. The area under the potential-time curve was found using a K and E compensating polar planimeter and the average potential was calculated from this area. This procedure was employed for several different percent duty cycles and for several different average cell currents, and in each case the potential recorded on the chart paper and the averaged potential calculated by the integration method were within the limits of accuracy of the latter method.

Average current under pulsed load was measured using a D.C. ammeter. Again, since the response time of the meter was much greater than the time of one cycle, the ammeter registered an average current. This average was checked by methods similar to those described above, i.e., by photographing oscilloscope traces of the potential across the load resistor, graphically integrating the area under these traces, and calculating the average current from this area knowing the value of the load resistor. Again, agreement was obtained which was within the limits of accuracy of the integration method.

*Model P1A, Parabam, Inc., Hawthorne, California.

RESULTS

Four cells were arranged in series in the pulse loading system as shown in Figure 2. The poorest of the cells were chosen for study since smaller currents were required to bring the cells into the region of concentration polarization. A voltage-current curve for one cell is given in Figure 3. The open circuit potential of this cell was 1.015 volt. This open circuit potential was characteristic of all the cells which were tested.

The cell was allowed to come to equilibrium potential under steady load, and then the pulsing circuit was activated and the cell allowed to equilibrate at the same average current. No change in potential under pulsed loading was observed until the currents reached the region where concentration polarization began to take effect. In this region a significant increase in performance was noted.

The cell reached an equilibrium potential of 0.340 volt under a steady 4.5 amp load. The results of pulsing at a 37.5 amp, 1000 c/s, 12% duty cycle (an average current of 4.5 amp) are shown in Figure 4. From a potential of 0.340 volt under steady load, the potential of the cell rose to 0.425 volt.

Equilibrium potential for the same cell under a 5 amp steady load was 0.075 volt. Pulsing the cell at 41.5 amp, 1000 c/s, 12% duty cycle (an average current of 5 amp) resulted in a potential of 0.300 volt. This behavior is shown in Figure 5.

Attempts were made to observe any increase at other frequencies and duty cycles. Changing duty cycle or frequency, however, necessitated changing the value of C_2, the voltage of the power supply, and the resistance of the load if the same average current was to be maintained. An attempt to change these three nearly always resulted in instability of the system since they could not be changed simultaneously. Because of the instability, SCR_1 remained on or off and the cell decayed or recovered rapidly. When stability was regained at the new duty cycle or frequency, the cell often would not return to the same potential at the average current selected. Efforts are now being made to correct this situation so that the parameters, duty cycle and frequency can be studied.

Oscilloscope photographs of cell potential during pulsing were taken while the cell was subjected to a 5 amp average current. The pulse which turns off SCR_1 can be seen on reproductions of each of these photographs (Figure 6). The width of this pulse is 20μ sec.

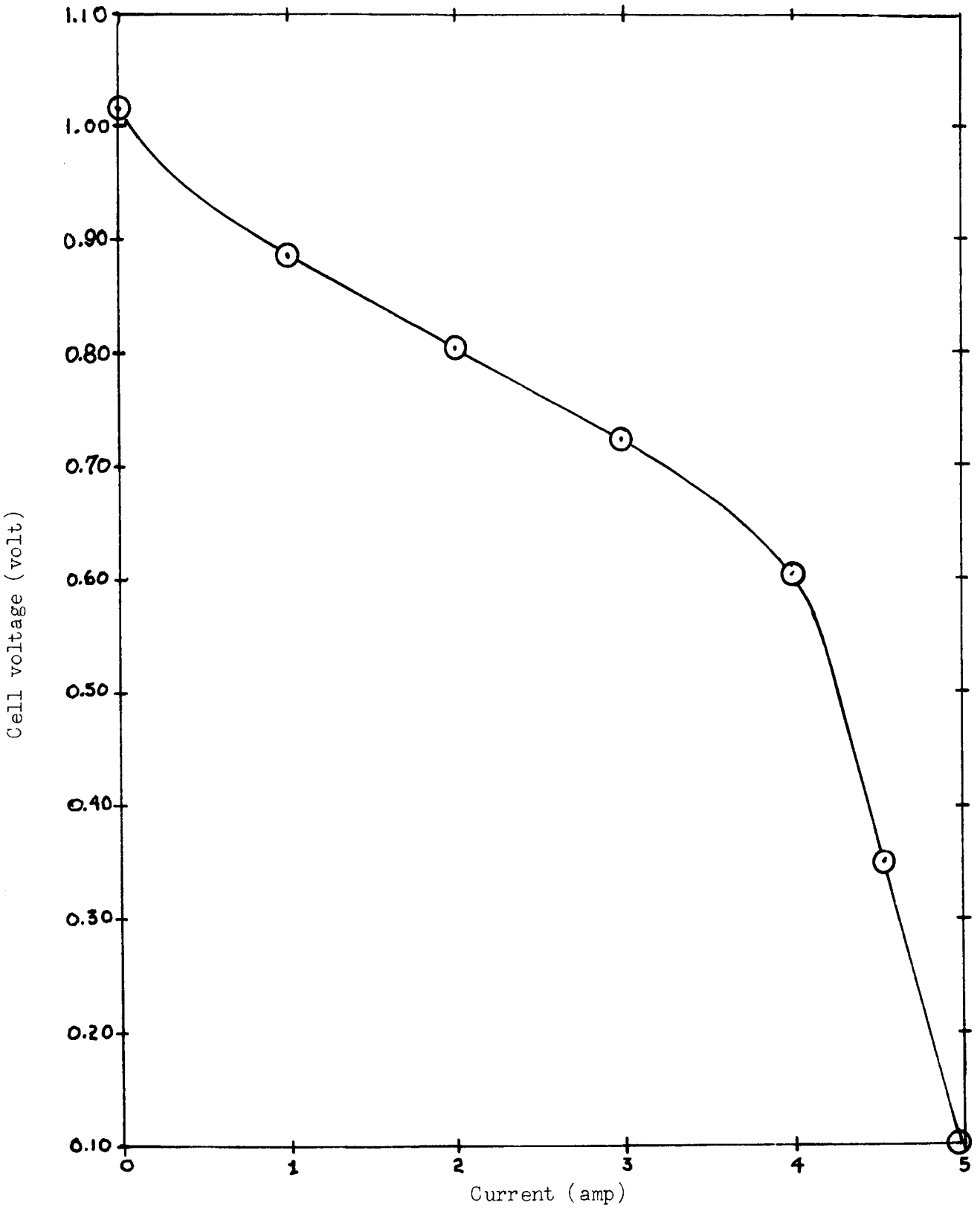

Figure 3. Voltage-current curve for cell.

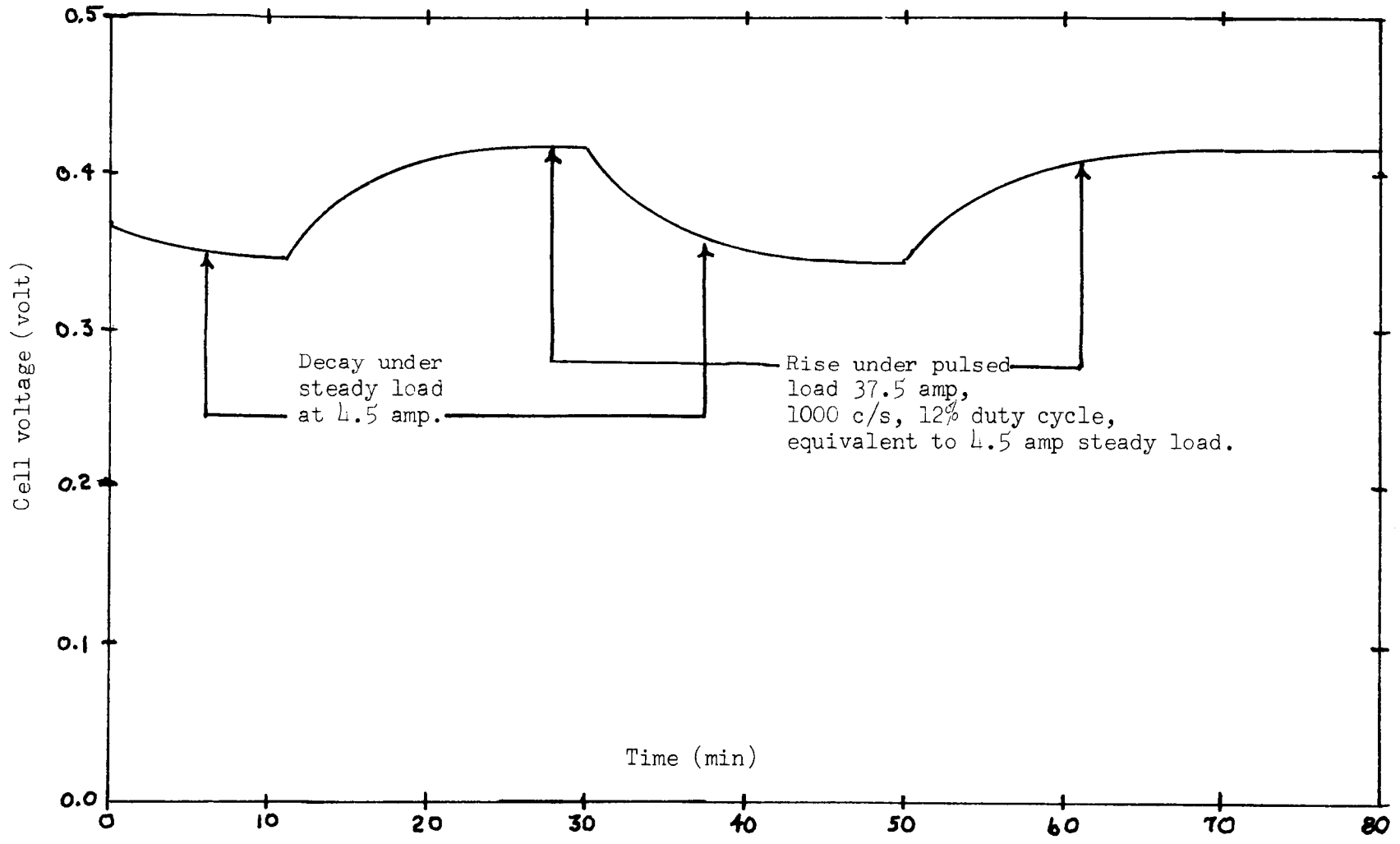

Figure 4. Cell voltage under pulsed and steady load.

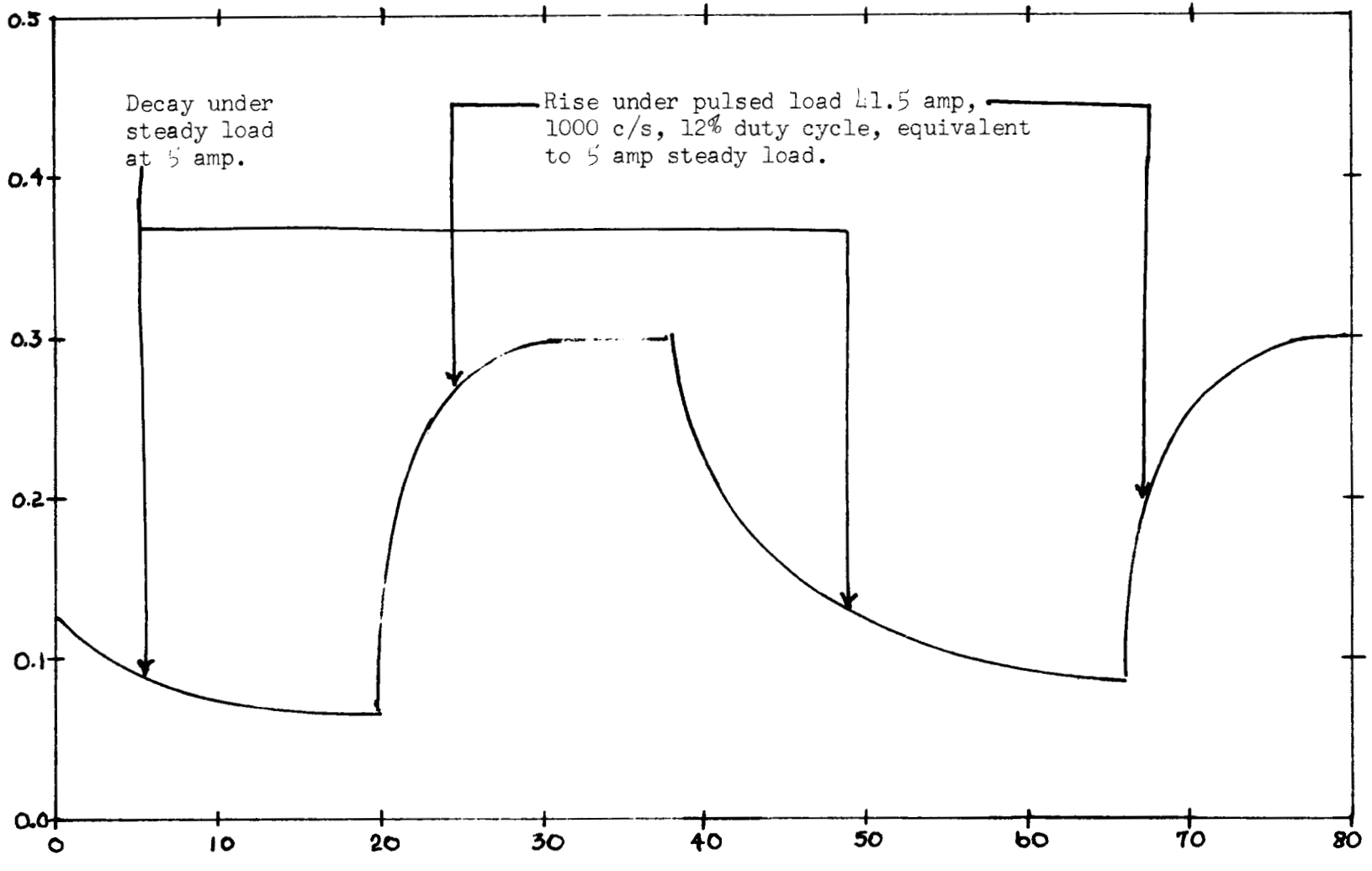

Figure 5. Cell voltage under pulsed and steady load.

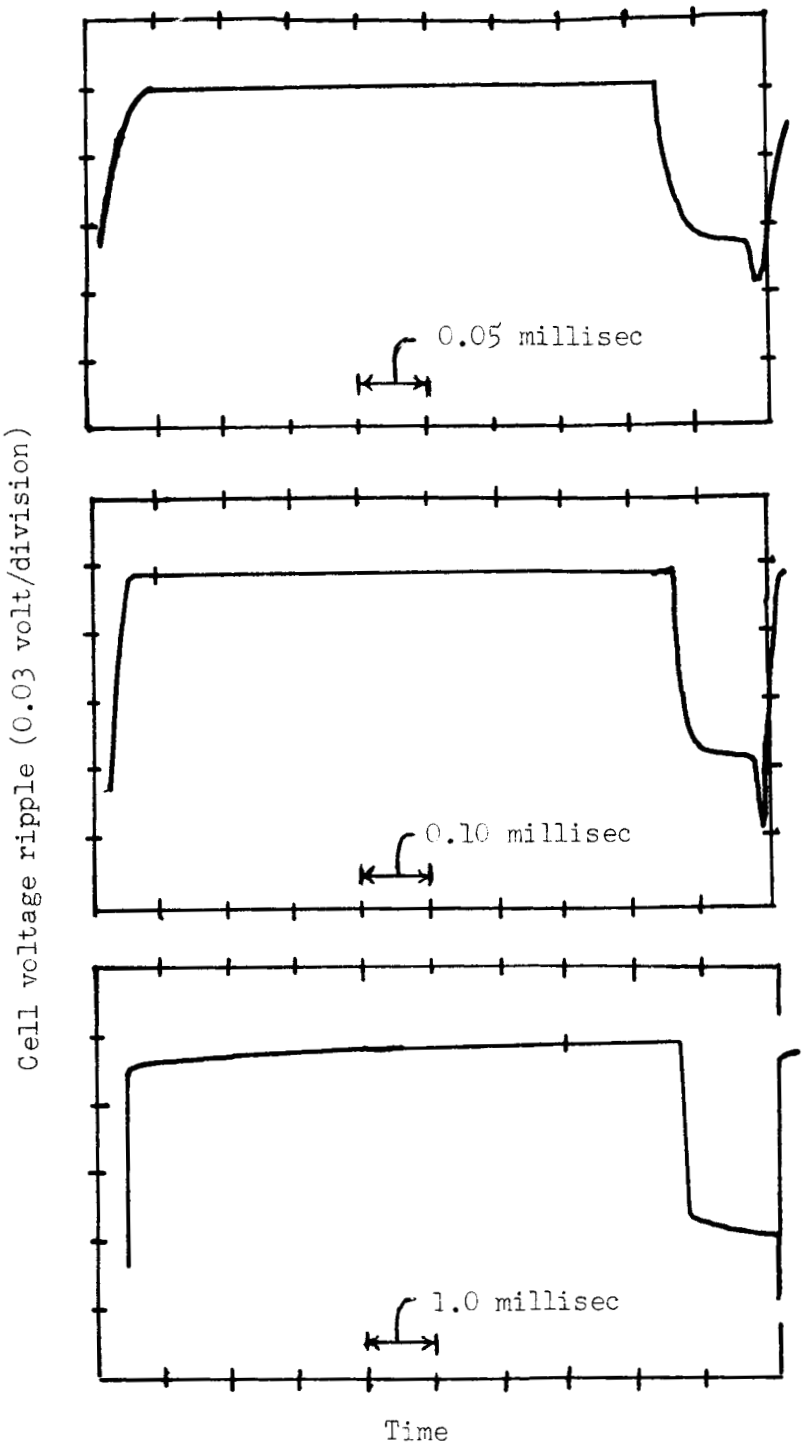

2000 c/s, 41.6 amp,
0.03 volt/cm,
12% duty cycle,
equivalent to 5 amp
steady load.

1000 c/s, 41.6 amp,
0.03 volt/cm,
12% duty cycle,
equivalent to 5 amp
steady load.

100 c/s, 41.6 amp,
0.03 volt/cm,
12% duty cycle,
equivalent to 5 amp
steady load.

Figure 6. Voltage ripple for cell at various frequencies for average current of 5 amp.

PART II

APPLICATION OF GALVANOSTATIC STUDIES TO FUEL CELL ELECTRODES

ABSTRACT

Galvanostatic curves reflect the presence of adsorbed or chemically combined species at an electrode surface, the nature and detailed characteristics of the electrical double layer, and an exact thermodynamic description of the condition at the electrode at all times. Application of this technique to fuel cell electrodes has facilitated the study of catalytic treatment and permitted the optimizing of electrode treatment as well as providing a rapid technique for qualitative screening of electrodes before introduction into a working fuel cell.

On the fundamental side, a detailed study of the palladium-gold system has emphasized the importance of unpaired d-electrons in the catalyst, and a study of the platinum-palladium system has facilitated the development of an optimum performance electrode while simultaneously providing an explanation for its efficiency in a practical fuel cell.

INTRODUCTION

Most of the available electrochemical data on operational cells relates to steady state conditions. Even under these conditions, the steady state (non-equilibrium) thermodynamic considerations are imperfectly understood and the condition of the electrodes ill defined. Since the majority of fuel cells are required to operate into varying and often pulsed load, typically a solid state inverter, it is imperative to examine the electrochemical characteristics of fuel cells under these conditions. To effect such a study two approaches possess particular merit: the direct characterization of fuel cells under pulsed loading conditions considering each electrode simultaneously but separately against a standard reference electrode and the application of galvanostatic techniques either in a working cell or a simulated system. The former approach yields data of direct applicational importance but cannot resolve the more complex details whereas the latter technique, now to be described, leads to more fundamental data and to a better understanding of the inherent electrochemical features of cells under operational conditions.

The galvanostatic technique is well known and is excellently described in numerous standard texts[1,2] and will not be reviewed at this juncture. This investigation is divided between the application of galvanostatic techniques to operational fuel cell electrodes and to the separate investigation of the fundamental aspects of fuel cell electrode catalysts.

I. INVESTIGATION OF OPERATIONAL FUEL ELECTRODES

EXPERIMENTAL

Since this study relates to the application of the galvanostatic technique to fuel cell electrodes, it was imperative to establish experimental procedures that yield highly reproducible results. For this reason, a single substrate of uniform porosity sintered nickel has been selected. It is not inferred that this is the optimum substrate but it has been separately established that the technique yields data which are especially applicable to other types of electrodes. On this same basis, no attempt has been made to optimize performance or to investigate variations in electrolyte, operating conditions or cell geometry.

The electrode material consisted of a nickel wire mesh covered with porous sintered nickel. Electrolytically deposited platinum black, palladium black, and a co-deposit of the two were employed as catalysts. The concentration of impregnation solutions, the method of impregnation and the time of platinizing or palladizing were parameters which were studied.

The sintered nickel electrodes were washed in distilled water in an ultrasonic bath and were then impregnated in the bath with solutions of platinum chloride, palladium chloride or both. Electrolytic reduction was effected with a plating current of 45 ma/cm^2 for various periods of time in a solution of the desired catalyst salt or salts which contained 0.1% lead acetate. The platinized, palladized or co-deposited electrodes were very thoroughly rinsed with distilled water before the galvanostatic measurements were made. The electrolyte (30% potassium hydroxide, carbonate free) was heated to boiling to remove dissolved oxygen and cooled under dry nitrogen.

To supply the constant current necessary for galvanostatic work, the constant current generator shown in Figure 7a was developed. This generator is a hybrid circuit composed of three general sections, a 300-volt power supply, a reference power supply, and a current set configuration. A simplified diagram of the three sections is given in Figure 7b. The series combination of tube and transistor provides high gain resolution over a wider range of compliance voltages than would be possible with the transistor alone and has better regulation than could be obtained from the tube alone over the range of 10 μa to 100 ma.

Transistor Q_1 holds the voltage across the current setting Varley Potentiometer to a value approximately equal to the temperature compensated Zener diode reference source of 6.3 volts and determines the magnitude of the emitter current. Since α for transistor Q_1 is essentially unity, its collector current and the current through the cathode of tube V_1 are equal to the emitter current. The collector voltage of Q_1 automatically adjusts to provide the necessary bias for the grid of V_1 depending on the plate voltage supplied by the 300-volt power source as affected by the load.

In preparation for galvanostatic measurements, the electrode under study was immersed in a freshly prepared electrolyte solution and the constant current generator was connected between this electrode and a platinum gauze counter electrode. A known current was passed through the thermostated cell which contained these electrodes. The potential between the electrode under study and a mercury-mercury oxide (30% potassium hydroxide) reference electrode was followed by means of a potential divider and a recorder.

The electrode was cathodically polarized to hydrogen evolution and the direction of current flow was reversed to observe the anodic charging curve. Three definite regions on the anodic potential-time curve were noted as the potential of the electrode increased to oxygen evolution. These were: (a) region in which hydrogen is present on the surface; (b) region of electrical double-layer charging; and (c) region in which oxides or chemisorbed oxygen is present on the surface.[3,4]

Figure 7.a. Constant Current Generator Circuit

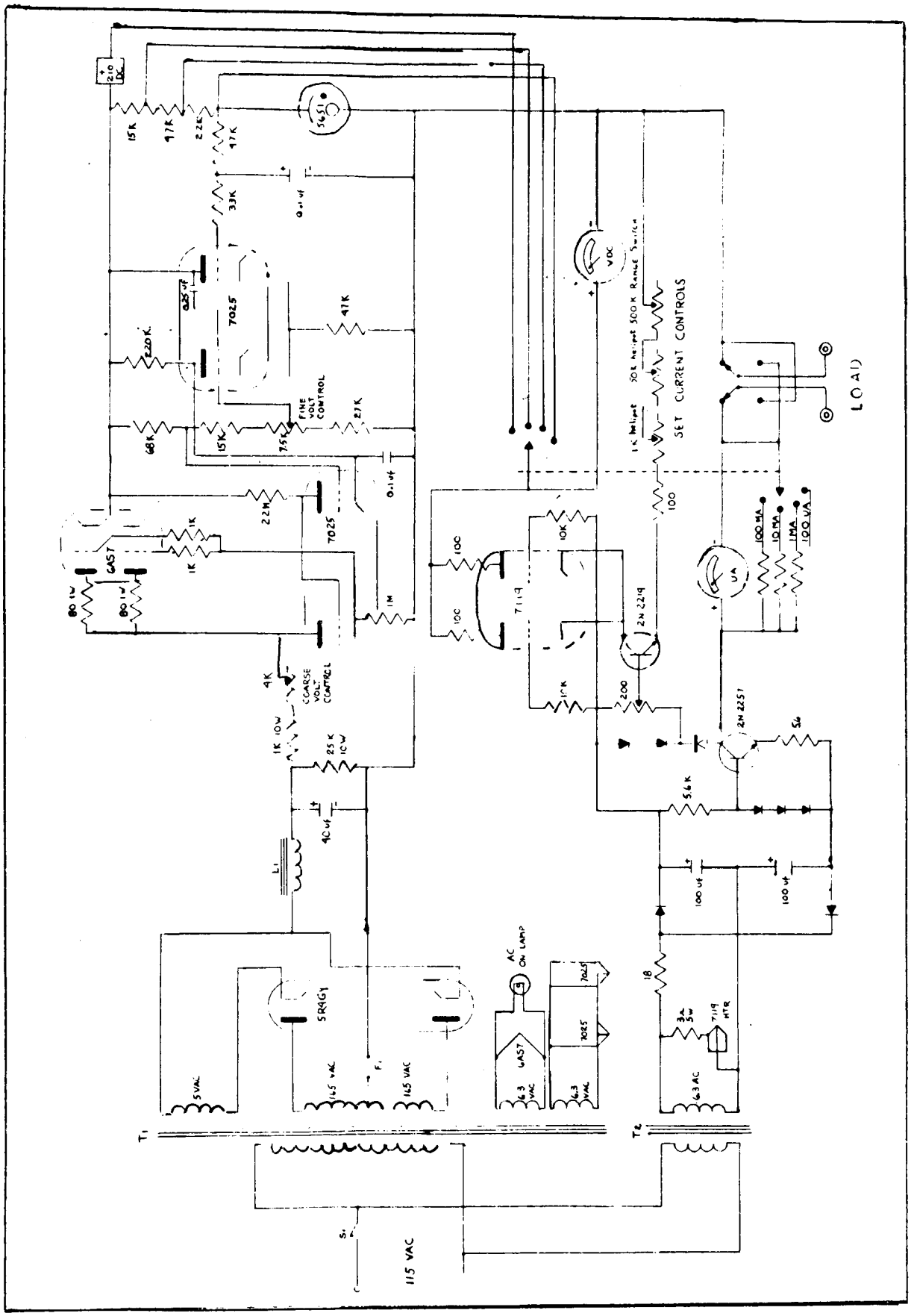

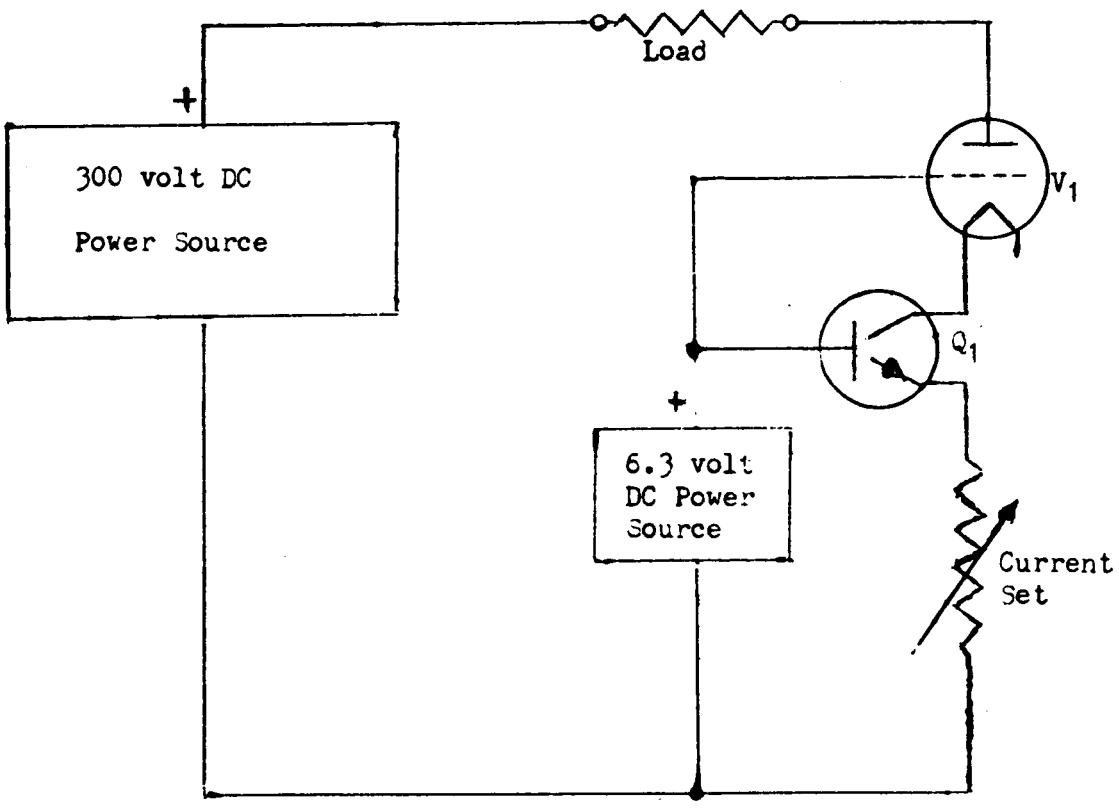

Figure 7b. Simplified Diagram of Constant Current Generator

Figure 8. Galvanostatic Anodic Charging Curves for Electrodes.

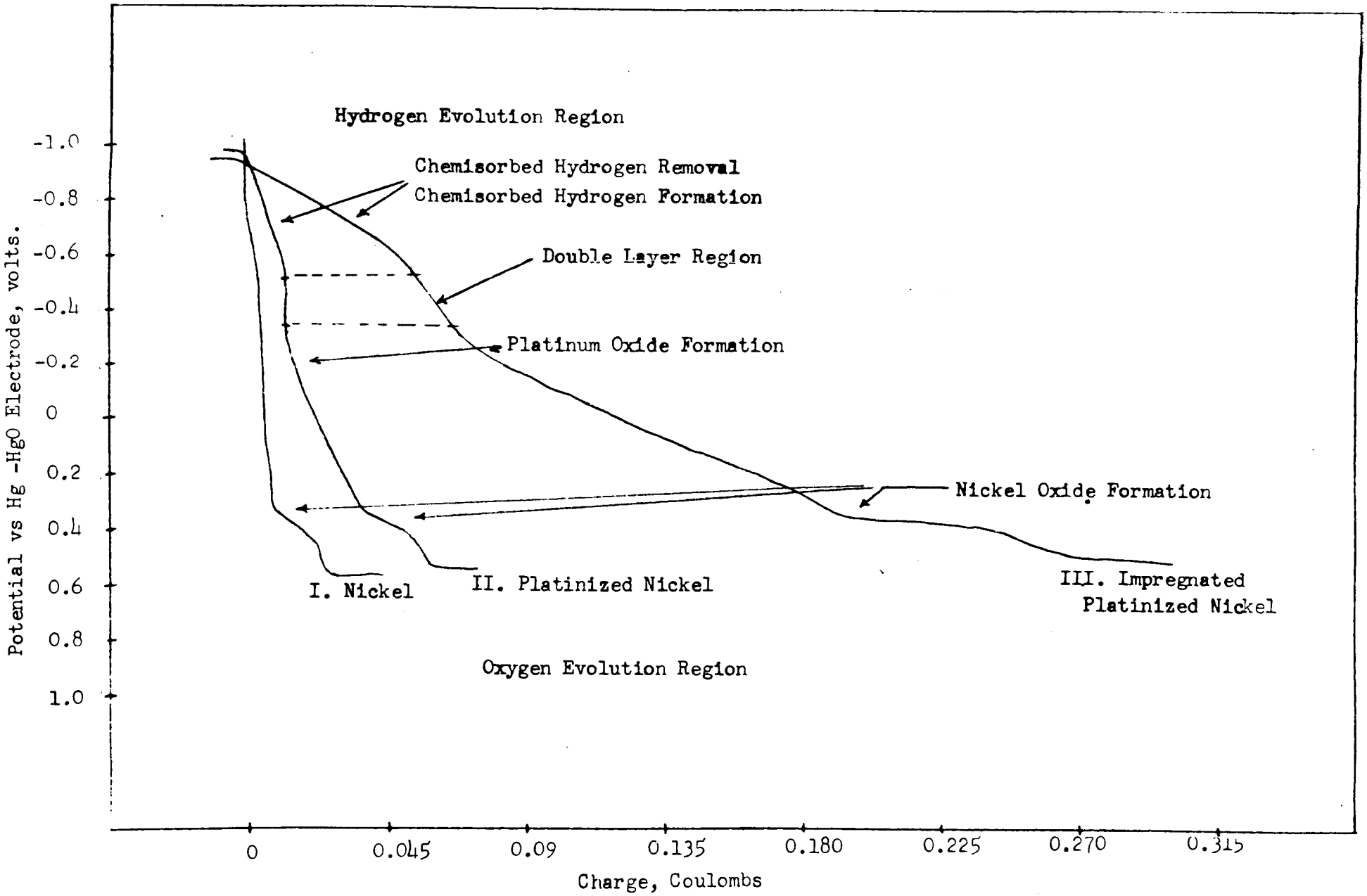

The time required to discharge the sorbed hydrogen was especially noted along with the slope of the double-layer region. The capacitance of the electrical double-layer, $\Delta Q/\Delta V$, can be related to the active electrochemical surface area of the electrode.[3,4]

RESULTS

The sintered nickel and platinized sintered nickel electrodes were the first to be studied galvanostatically. Curve I in Figure 8 was obtained using a sintered nickel electrode with a geometric area of 2 cm^2. Platinization of this electrode for 5 minutes at 45 ma/cm^2 in a 4% chloroplatinic acid solution approximately doubled the capacitance of the double-layer region and effected a chemisorption of hydrogen on the electrode; this behavior is shown in Curve II. Curve III was obtained using an electrode which had been placed in an ultrasonic bath for 5 minutes in a 4% chloroplatinic acid solution prior to platinization. This treatment greatly increased the double-layer capacitance and the amount of chemisorbed hydrogen. Further platinization for 10, 15, and 20 minutes showed that there was little change in the amount of hydrogen chemisorbed on the surface or in the capacitance of the double layer. Calculations of the amount of chemisorbed hydrogen and the capacitance of the double layer based on Figure 8 are given in Table I.

Table I

Electrode	Atoms of H on Surface	Calculated Capacitance of Double-Layer (Farads)
Ni		0.050
Ni, platinized for 5 minutes	1.25×10^{18}	0.175
Ni, impregnated with PtCl, then platinized for 5 minutes	4.5×10^{18}	1.200
10 minutes	4.78×10^{18}	1.125
15 minutes	4.5×10^{18}	0.965
20 minutes	4.87×10^{18}	1.080

Surface areas were calculated from the capacitance of the double-layer using a rough conversion factor of 1 cm^2 = 150 μF capacitance (a value given for shiny platinum[3]). Surface areas were also calculated from the amount of hydrogen on the surface

assuming a 1:1, H:Pt ratio and a surface area of 7.6×10^{-16} cm^2/Pt atom on the (1, 0, 0) crystal plane. Table II compares the two calculated surface areas.

Table II

Electrode	Surface Area by H on Surface	Surface Area by Capacitance of the Double-Layer
Ni, platinized for 5 minutes		900 cm^2
Ni, impregnated with $PtCl_4$, then platinized for 5 minutes	3420 cm^2	7500 cm^2
10 minutes	3700 cm^2	6860 cm^2
15 minutes	3420 cm^2	5360 cm^2
20 minutes	3700 cm^2	6000 cm^2

A surface area of 0.2 m^2/g was measured for the sintered nickel electrode by nitrogen adsorption using the continuous flow method.[5] By weighing the electrodes employed in the galvanostatic measurements and calculating a total surface area from the above figure, a value of 400 cm^2 was obtained. If the relation between surface area and double-layer capacitance of nickel is about 1 cm^2 = 30 μF, a surface area of 900 cm^2 is calculated, which is a little more than double the B.E.T. area.

Assuming that the double-layer capacitance is an approximate measure of the surface area, it can be seen that platinization for five minutes does not significantly increase the active surface area of the electrode (Table II). After the platinum chloride solution was impregnated into the pores of the nickel electrode ultrasonically, however, platinization rapidly increased the surface area which then leveled off as a function of time in the ultrasonic bath. The reasons for the discrepancies between the results of the two methods of calculation can possibly be attributed to three factors:

1. The surface area of the electrode would appear to be higher than calculated from hydrogen adsorbed on the surface if the surface hydrogen-platinum ratio were less than 1:1.

2. If the removal of the chemisorbed hydrogen on the surface extended into the double-layer region, the effect would produce a higher $\Delta Q/\Delta V$ ratio and, hence, a higher apparent capacitance of the electrical double layer. The surface area would then appear to be higher than it actually is.

3. The value for the double-layer capacitance as a function of actual surface area is greater than assumed. This, in fact, has been substantiated by determining the specific capacitance against current density.

Extensive studies were performed on the effect of platinization time and time of impregnation in the ultrasonic bath on double-layer capacitance. For these studies, a new nickel electrode was employed for each run.

Figure 9 shows the effect of time in the ultrasonic bath on capacitance of the double layer. Each of the electrodes was platinized for one minute. One minute in the ultrasonic bath significantly increased the capacitance, but not in proportion to the time and electricity expended. After five to ten minutes treatment, excessive agitation in the ultrasonic bath resulted in physical deterioration of the electrodes. For this reason, shorter impregnation times are preferable.

Figure 10 shows the effect of platinization time on the capacitance of the double layer. Each electrode in this series was impregnated in the ultrasonic bath for two minutes prior to platinization. Increasing the platinization time above one minute had very little effect on the capacitance of the electrical double layer. Similar behavior was observed on electrodes for replatinization times up to twenty minutes.

In summary, impregnation time in the ultrasonic bath had a considerable effect on the surface area of a platinum-palladium catalyst, but after five minutes led to deterioration of the nickel electrode. Platinization time, after one minute, had little effect. Maximum effective catalyst area, therefore, appears to be obtained at the indicated platinization current densities, when the impregnation time is in the vicinity of four to five minutes and platinization time is about one minute.

Galvanostatic studies were performed on the following electrodes:

1. Standard sintered nickel.
2. 1%:4% Pd:Pt co-deposit.
3. 2%:4% Pd:Pt co-deposit.
4. 3%:4% Pd:Pt co-deposit.
5. 4%:4% Pd:Pt co-deposit.

Figure 9. Double-Layer Capacitance vs Impregnation Time

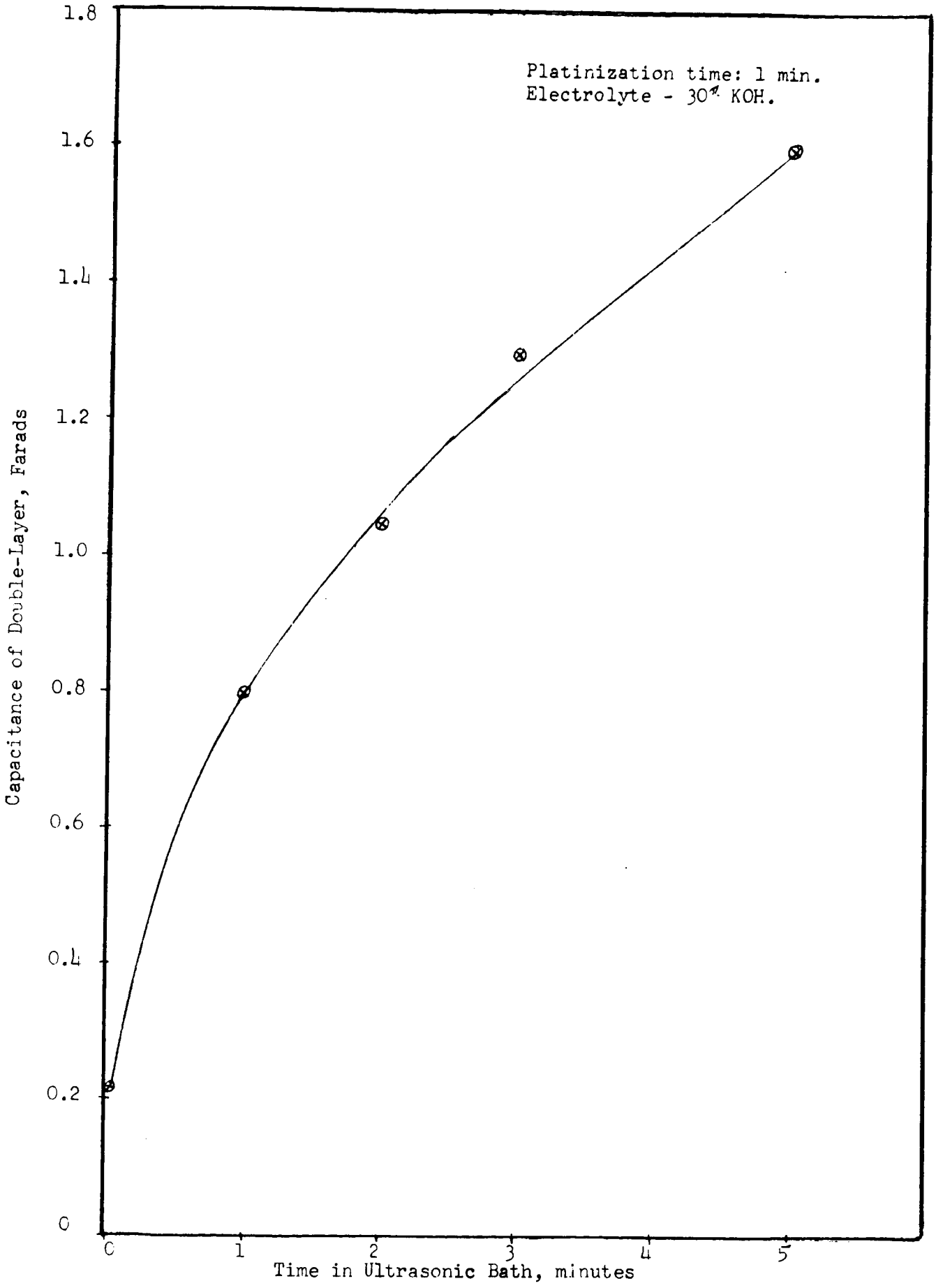

Figure 10. Double-Layer Capacitance vs Platinization Time

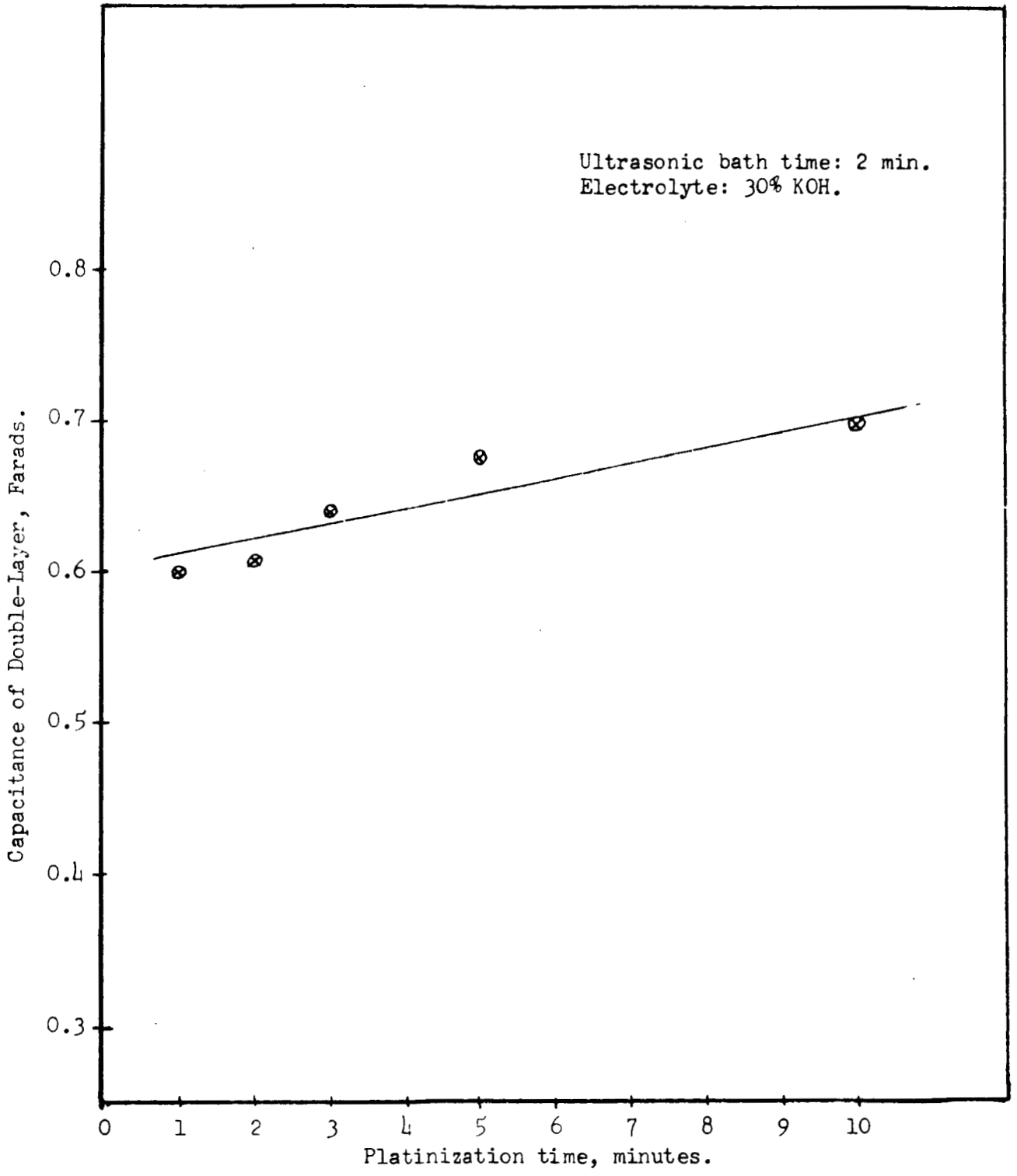

These studies were performed at 25°C with a polarizing density of 10 ma/cm^2.

Results of the galvanostatic anodic charging curves are shown in Figure 11. AC represents the hydrogen-ionization steps in all three cases. In Curves 1 and 2, the change in potential with quantity of electricity passed is virtually the same. Steps AB, which represent the hydrogen on the surface which will support a high potential, are also equivalent. On Curve 3, however, it is seen that step AB is extended to more than twice the length that it is on Curves 1 and 2. The hydrogen ionization step appears to support a higher potential on Curve 3 for the passage of a larger quantity of electricity. No significant difference in the double-layer capacitances was evident, but the overall amount of hydrogen participating in the hydrogen-ionization step increased with the palladium content of the platinizing-palladizing solution at these concentrations.

Galvanostatic studies on platinum-palladium alloy wires show results similar to those obtained on the co-deposits. The anodic discharge steps for hydrogen chemisorbed on the surface and adsorbed in these alloys are extended considerably over those found for a platinum electrode. The 50% platinum-50% palladium alloy will anodically discharge about 400 times as much hydrogen as platinum with less than 0.1 volt polarization at low current densities.

Discharge curves for the hydrogen electrode in a fuel cell (Figure 12) show clearly the superiority of the platinum-palladium co-deposited catalyst over platinum. The galvanostatic results above corroborate these data. Considerably more hydrogen is available for discharge at low polarization in the co-deposits.

II. GALVANOSTATIC INVESTIGATION OF PALLADIUM-GOLD ALLOYS

In order better to understand the absorption of hydrogen on palladium, galvanostatic studies were then performed on a series of palladium-gold alloys. Several authors[4,6] have observed a three-stage process in the anodic charging curves occurring at the surface of a palladium electrode which had previously been subjected to hydrogen evolution. The first stage is an irregular change in potential which occurs during the ionization of hydrogen at the surface; the second is a linear change in potential which represents the charging of the electrical double layer; the third is the potential change which represents the formation of oxides or hydroxides at the surface which occurs before oxygen evolution.

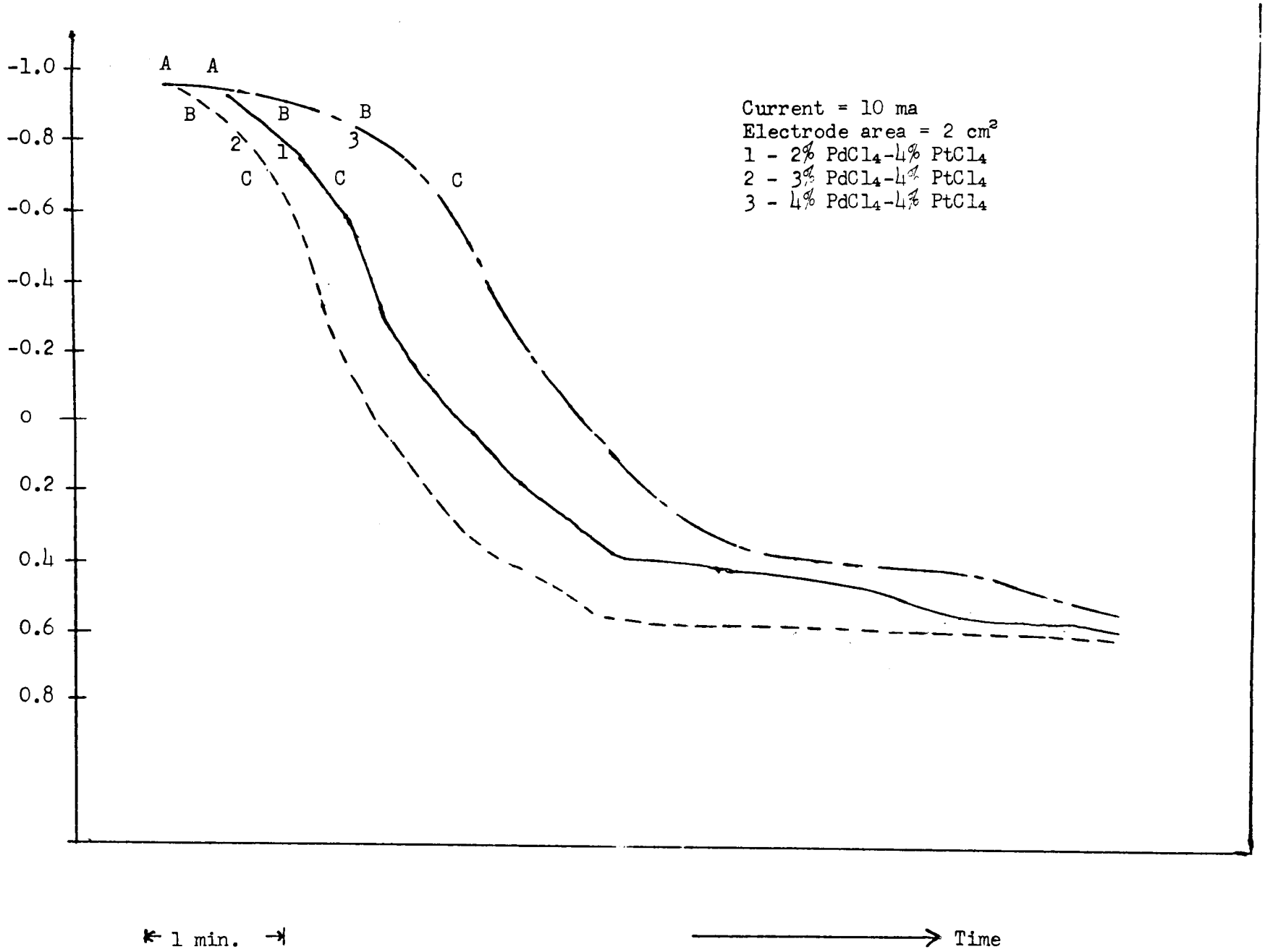

Figure 11. Galvanostatic Studies of Several Catalyzations of Clevite Nickel

Figure 12. Hydrogen and Oxygen Electrode Discharge Curves

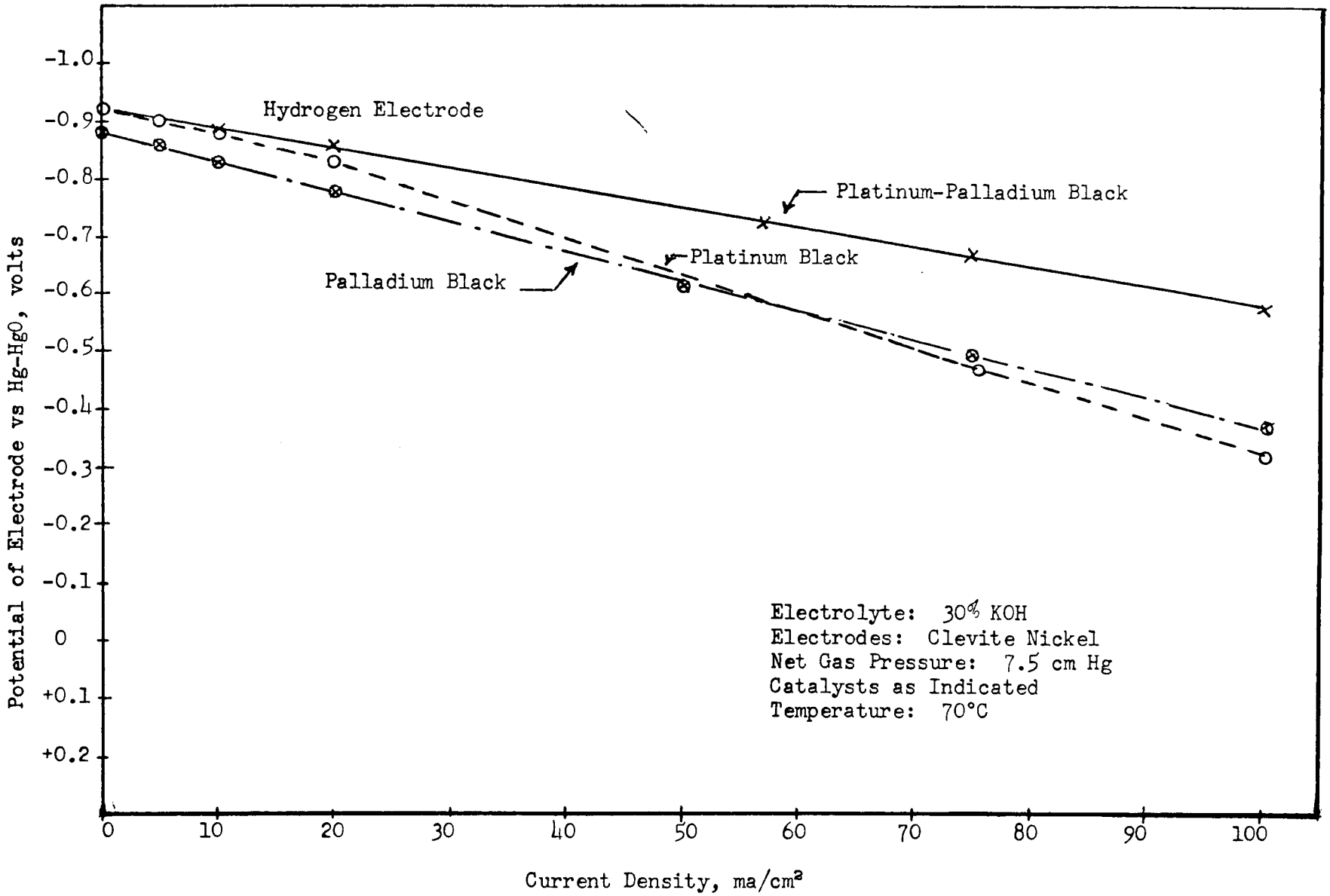

On gold surfaces[7,8,9] only the latter two of the above three stages are observed. No hydrogen ionization is detected indicating that no chemisorption of hydrogen has taken place.

Work[10,11] on the chemisorption of hydrogen and on p-hydrogen conversion has shown the importance of the electronic structure of the metal. In view of these results, investigation commenced with a study of the relationship between electronic structure and the charging curves for a series of palladium-gold alloys.

EXPERIMENTAL PROCEDURES

A series of high-purity annealed alloy wires were obtained with the following compositions of gold by weight: 20%, 40%, 60%, 75% and 80%. Seventy-five percent gold corresponds to a 62:38 gold: palladium atomic ratio. The 60:40 gold:palladium ratio is the composition at which the d-band of the alloy is filled and where, in p-hydrogen conversion reactions,[11] a rapid increase in activation energy is found to occur. The alloys were investigated in deoxygenated 1N sulfuric acid electrolyte using the galvanostatic apparatus in the previous section.

RESULTS

A preliminary summary of these results has been published by Gray et al.[12] The results for palladium and gold correspond closely to those previously reported[4,6,7,8,9] and is illustrated in Figure 13. With palladium, a hydrogen ionization step is observed following cathodic polarization at hydrogen evolution, the length of the step depending on the time spent at hydrogen evolution. With gold, the hydrogen ionization step is absent or, in a very few cases where hydrogen evolution is maintained for long periods of time, is very small.

Alloys richer than 60 atomic percent gold show no detectable hydrogen on the surface and behave much like gold. Alloys with less than 60 atomic percent gold show an appreciable hydrogen ionization step indicating that much hydrogen has been sorbed; these alloys behave much like palladium. It would appear, then, that the change in affinity of these alloys for palladium occurs at about the alloy composition where the d-band is just filled, i.e., unpaired d-electrons seem to be necessary for the chemisorption of any appreciable quantity of hydrogen.

A very important effect has been noted in the galvanostatic investigation of platinum-palladium and palladium-gold alloys. For palladium and the alloys which normally chemisorb and absorb hydrogen, no hydrogen can be detected by anodic charging curves until

Figure 13. Anodic Charging Curves for Palladium-Gold Alloys

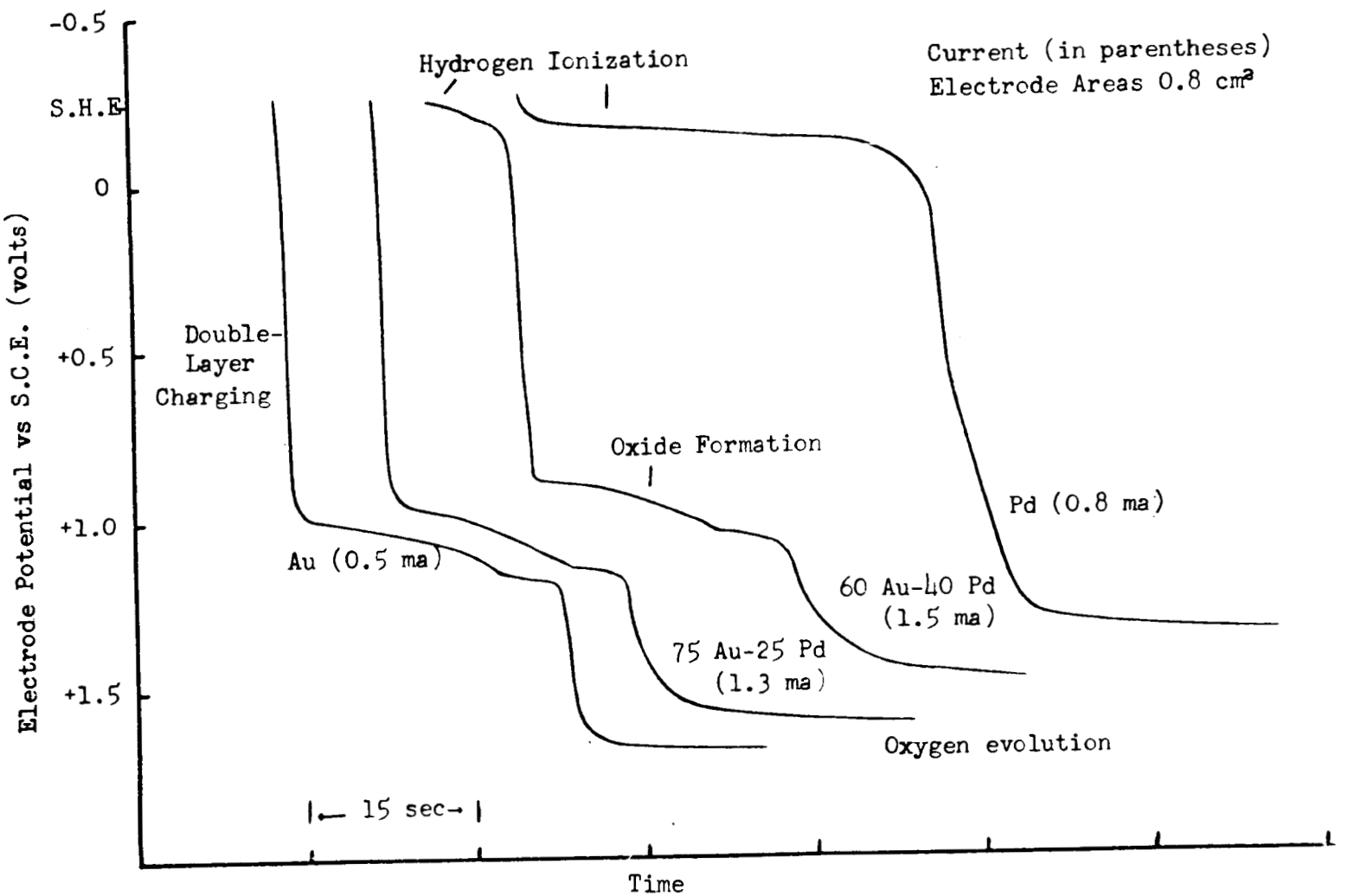

the potential of the first surface oxide is exceeded and the electrode recycled through cathodic and then anodic charging. In Figure 14, it can be seen that no hydrogen discharge step is present as long as the first oxide is not present. As soon as the charging curves indicate that the oxide formation is complete for the particular polarizing current employed, and the electrode recycled, hydrogen appears to be chemisorbed and absorbed by the alloy. Results of previous investigators have indicated the necessity of extensive anodic polarization to activate surfaces toward hydrogen chemisorption.[13,14] In some cases, the presence of an initial passivating film of hydrogen is theorized.[13] The results of this research support these views but further indicate that it is necessary only to exceed the potential of the first oxide layer to produce hydrogen on the surface and in the bulk which will support an electrochemical hydrogen ionization step. The above results will be applied to platinum-palladium catalyzed hydrogen electrodes in fuel cells.

Further investigations on the nature of hydrogen ionization on platinum-palladium and palladium-gold alloys are being undertaken by measuring the change in resistance of the alloys as the potential is changed from that of hydrogen evolution to that of oxygen evolution. Initial results on palladium are similar to those reported in the literature.[13,14,15] Work is continuing on the alloys. When pure gold was used as the electrode, no resistance change was noted indicating that no hydrogen had diffused into the bulk of the gold. An alloy of 40% platinum-60% palladium showed a 1% change in resistance while an alloy of 80% gold-20% palladium showed a 5% change.

CONCLUSIONS

From these data it is clear that valuable information can be derived regarding the detailed operation of fuel cell electrodes in active cells and separately that the individual electrodes can be studied to optimize the catalyst. It is considered probable that this technique may also find useful application in a wide variety of studies to determine the nature of hydrocarbon electrode processes, electrolyte polarization in the vicinity of each electrode separately but simultaneously, and the effect of geometric consideration, pore size and pore size distribution.

Figure 14. Galvanostatic Curves for Palladium-Gold Alloy

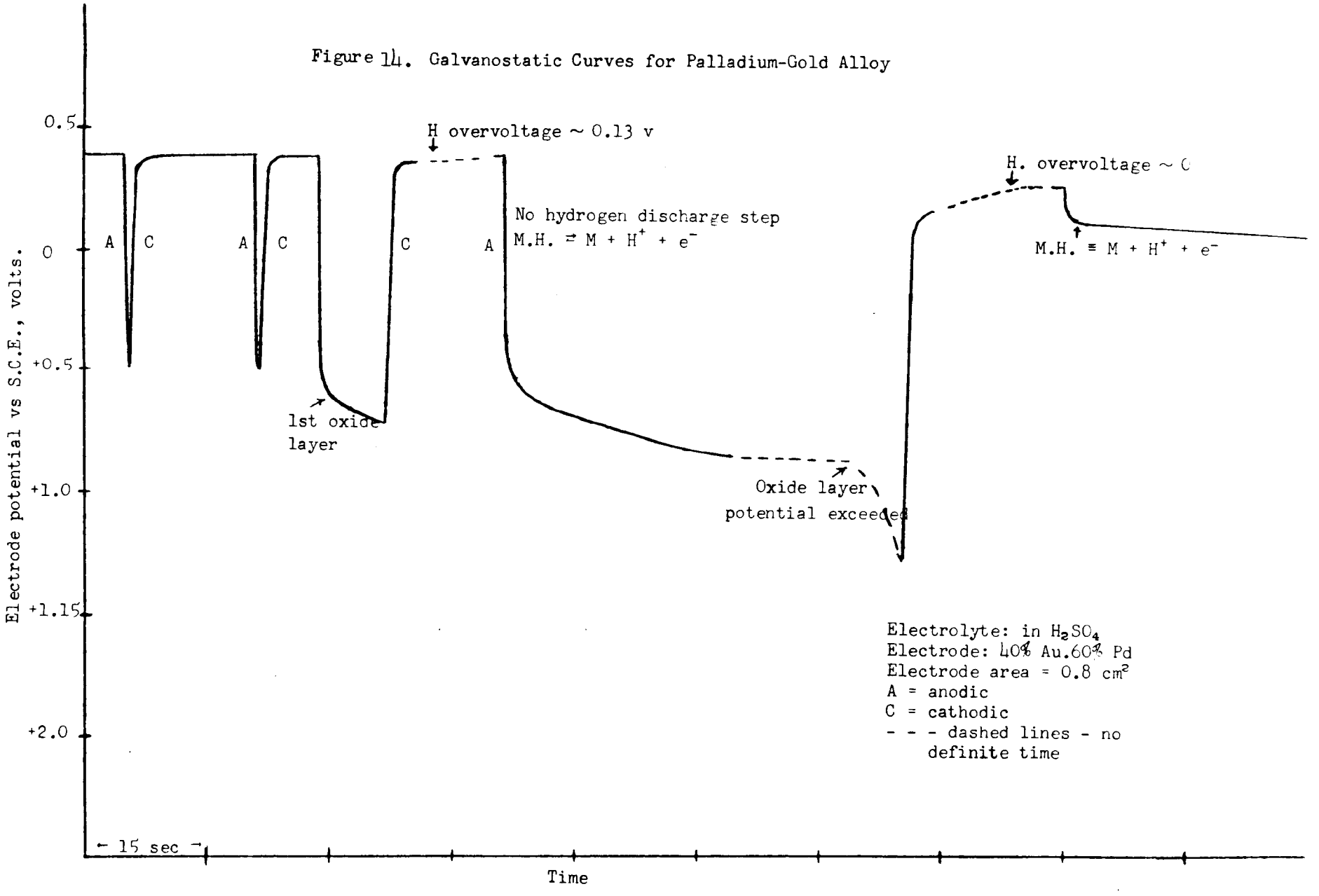

REFERENCES

1. Bockris, J. O'M., ed., Modern Aspects of Electrochemistry, vol. 1, Butterworths, London, 1954, pp. 139-142.

2. Delahay, P., ed., Advances in Electrochemistry and Electrochemical Engineering, vol. 1, Interscience, New York, 1961, pp. 254-265.

3. Hickling, A., Trans. Faraday Soc., 41, 33 (1945).

4. Hickling, A. and Vrjosek, G. G., Trans. Faraday Soc., 57, 123 (1961).

5. Eggertsen, F. T., Anal. Chem., 30, 1387-1390 (1958).

6. El Wakkad, S. E. S. and El Din, A. M. S., J. Chem. Soc., 3094 (1954).

7. Armstrong, G., Himsworth, F. R., and Butler, J. A. V., Proc. Roy. Soc., 143, A 89 (1933).

8. El Wakkad, S. E. S. and El Din, A. M. S., J. Chem. Soc., 3098 (1954).

9. Hickling, A., Trans. Faraday Soc., 42, 518 (1956).

10. Dowden, D., Chemisorption, ed. W. E. Garner, Butterworths (1957).

11. Couper, A. and Eley, D., Disc. Faraday Soc., 8, 172 (1950).

12. Gray, T. J., Rozelle, R. B. and Soeder, M. L., Nature, 202 [4928], 181-182 (1964).

13. Flanagan, T. B. and Lewis, F. A., Trans. Faraday Soc., 55, 1400 (1959).

14. Hoare, J. P., Schuldiner, S. and Castellan, G. W., J. Chem. Phys., 28, 22 (1958).

15. Smith, D. P., Hydrogen in Metals, University of Chicago Press (1948).

DISTRIBUTION LIST FOR FUEL CELL REPORTS - GRANT NsG-384

National Aeronautics and Space Administration
Washington, D. C. 20546
Attn: Miss Millie Ruda/AFSS-LD (3)
Walter C. Scott/RPP (1)
Ernst M. Cohn/RNW (1)
George F. Esenwein/MSA (1)
John L. Sloop/RP (1)
A. M. Andrus/FC (1)
Fred Schulman/RN (1)
Miss Winnie M. Morgan (25)

National Aeronautics and Space Administration
Goddard Space Flight Center
Greenbelt, Maryland
Attn: Thomas Hennigan (1)

National Aeronautics and Space Administration
Lewis Research Center
21000 Brookpark Road
Cleveland, Ohio 44135
Attn: B. Lubarsky Mail Stop 86-1 (1)
Martin J. Saari " " " (1)
Robert L. Cummings " " " (1)
Harvey J. Schwartz " " " (1)
William J. Nagle " " " (1)
N. D. Sanders " " 302-1 (1)
N. T. Musial " " 77-1 (1)

National Aeronautics and Space Administration
Marshall Space Flight Center
Huntsville, Alabama
Attn: Philip Youngblood (1)
Eugene Cagle (1)

National Aeronautics and Space Administration
Manned Space Craft Center
Houston, Texas 77001
Attn: William R. Dusenbury (1)
Systems Evaluation and Development Division
Rich Building, 6040 Telephone Road
Robert Cohen, Gemini Project Office

Jet Propulsion Laboratory
4800 Oak Grove Drive
Pasadena, California
Attn: Aiji Uchiyama (1)

DEPARTMENT OF THE ARMY

U. S. Army Engineer R and D Labs
Fort Belvoir, Virginia
Attn: Mr. B. C. Almaula (1)
Electrical Power Branch

U. S. Army Engineer R and D Labs
Fort Monmouth, New Jersey
Attn: David Linden (Code SELRA/SL-PS) (1)
Dr. Adelph Fischbach (Code SELRA/SL-PS) (1)
Arthur F. Daniel (Code SELRA/SL-PS) (1)

U. S. Army Research Office
Physical Sciences Division
3045 Columbia Pike
Arlington, Virginia
Attn: Dr. Sidney J. Magram (1)

Harry Diamond Labs
Room 300, Bldg. 92
Connecticut Avenue and Van Ness Street, N. W.
Washington, D. C.
Attn: Robert Goodrich (1)

U. S. Army Mobility Command
Research Division
Center Line, Michigan 48015
Attn: O. Renius (AMSMO-RR) (1)

U. S. Army Research Office
Box CM, Duke Station
Durham, North Carolina
Attn: Paul Greer (1)
Dr. Wilhelm Jorgensen (1)

Research Office
R and D Directorate
Army Weapons Command
Rock Island, Illinois 61201
Attn: G. Ransmith, Chief (1)

DEPARTMENT OF THE NAVY

Office of Naval Research
Department of the Navy
Washington, D. C. 20546
Attn: Dr. Ralph Roberts (1)
Dr. J. C. White (1)
H. W. Fox (Code 425) (1)

Bureau of Ships
Department of the Navy
Washington, D. C. 20546
Attn: Bernard B. Rosenbaum (Code 340) (1)
C. F. Viglotti (Code 660) (1)
James B. Trout (Code 660S) (1)
CDR Joseph W. Thornbury (Code 649) (1)

Naval Ordnance Laboratory
Department of the Navy
Corona, California
Attn: Mr. William C. Spindler (Code 441) (1)

Naval Ordnance Laboratory
Department of the Navy
Silver Spring, Maryland
Attn: Philip B. Cole (Code WB) (1)

DEPARTMENT OF THE AIR FORCE

Systems Engineering Group
RTD, AFSC, USAF
Wright-Patterson Air Force Base, Ohio 45433
Attn: George W. Sherman (1)
Robert L. Kerr (1)
James E. Cooper (1)
ASRCEM-1 (1)

AF Cambridge Research Lab
Attn: Crze (1)
L. G. Hanscom Field
Bedford, Massachusetts
Attn: Francis X. Doherty (1)
Edward Raskind (Wing F) (1)
Commander (CRO) (1)

Rome Air Development Center, ESD
Griffiss AFB, New York
Attn: Commander (RAALD) (1)
Frank J. Mollura (RASSM) (1)

Hq., USAF (AFRST-PM)
Washington, D. C. 20546
Attn: LT COL William G. Alexander (1)

CAPT William H. Ritchie (1)
Sapece Systems Division
Attn: SSZAE-11
Air Force Unit Post Office
Los Angeles, California 90045

CAPT William Hoover (1)
Air Force Ballistic Missile Division
Attn: WEZYA-21
Air Force Unit Post Office
Los Angeles, California 90045

ADVANCED RESEARCH PROJECTS AGENCY

Mr. Charles F. Yost (1)
Asst. Director, Material Sciences
Advanced Research Projects Agency
The Pentagon, Room 3E 153
Washington, D. C. 20546

Dr. John H. Huth (1)
Advanced Research Projects Agency
The Pentagon, Room 3E 157
Washington, D. C. 20546

ATOMIC ENERGY COMMISSION

U. S. Atomic Energy Commission (1)
Auxiliary Power Branch (SNAP)
Division of Reactor Development
Washington, D. C. 20546

LT COL John H. Anderson (1)
Advanced Space Reactor Branch
Division of Reactor Development
U. S. Atomic Energy Commission
Washington, D. C. 20546

OTHER GOVERNMENT AGENCIES

Defense Documentation Center Hq. (1)
Cameron Station, Bldg. 5
5010 Duke Street
Alexandria, Virginia 22314
Attn: TISIA

Office, DDR&E: USW & BSS
The Pentagon
Washington, D. C. 20546
Attn: G. B. Wareham (1)

Institute for Defense Analyses
R&D Support Division
1666 Connecticut Avenue, N. W.
Washington, D. C. 20549
Attn: Dr. George C. Szego (1)

Power Information Center (1)
University of Pennsylvania
Moore School Building
200 South 33rd Street
Philadelphia, Pennsylvania 19104

Office of Technical Services (1)
Department of Commerce
Washington, D. C. 20009

PRIVATE INDUSTRY

American Cyanamid Company
1937 W. Main Street
Stamford, Connecticut 06901
Attn: Dr. R. G. Haldeman (1)

Allis-Chalmers Mfg. Co.
110 S. 70th Street
Milwaukee, Wisconsin 53201
Attn: Dr. T. G. Kirkland (1)

Allison Division of General Motors
Indianapolis, Indiana 46206
Attn: Dr. Robert E. Henderson (1)

Astropower, Inc.
2968 Randolph Avenue
Costa Mesa, California 92629
Attn: Dr. Carl Berger (1)

Battelle Memorial Institute
Columbus, Ohio 43201
Attn: Dr. C. L. Faust (1)

Bell and Howell Research Center
360 Sierra Madre Villa
Pasadena, California
Attn: Alan G. Richards (1)

Bell Telephone Laboratories, Inc.
Murray Hill, New Jersey 07971
Attn: Mr. U. B. Thomas (1)

Electrochemica Corp.
1140 O'Brien Drive
Menlo Park, California 94025
Attn: Dr. Morris Eisenberg (1)

Electro-Optical Systems, Inc.
300 North Halstead Street
Pasadena, California
Attn: Dr. Joseph Neustein (1)

Engelhard Industries, Inc.
497 Delancy Street
Newark, New Jersey 07105
Attn: Dr. J. G. Cohn (1)

ESSO Research and Engineering Company
Products Research Division
P. O. Box 215
Linden, New Jersey 07036
Attn: Dr. Carl Heath (1)

Ford Motor Company
Aeronutronics Division
Newport Beach, California
Attn: Dr. R. C. Bean (1)

General Electric Company
Direct Energy Conversion Operations
Lynn, Massachusetts
Attn: Dr. E. Oster (1)

General Electric Company
Research Laboratory
Schenectady, New York
Attn: Dr. H. Liebhafsky (1)

General Electric Company
Missile & Space Vehicle Dept.
P. O. Box 8555
Philadelphia, Pennsylvania 19101
Attn: A. D. Taylor (1)

Globe-Union, Inc.
900 East Keefe Avenue
Milwaukee, Wisconsin 53201
Attn: Dr. C. K. Morehouse (1)

Hoffman Electronics Company
Research Laboratory
Santa Barbara, California
Attn: Dr. Joseph Smatko (1)

Johns Hopkins University
Applied Physics Laboratory
8621 Georgia Avenue
Silver Spring, Maryland
Attn: W. A. Tynan (1)

Leesona-Moss Laboratories
Lake Success Park
Community Drive
Great Neck, New York
Attn: Dr. A. Moos (1)

Lockheed Missiles & Space Company
Sunnyvale, California 94086
Attn: Dr. George B. Adams (1)

Livingston Electronic Corporation
Route 309
Montgomeryville, Pennsylvania 18936
Attn: William F. Myers (1)

McDonnell Aircraft Corporation
Attn: Project Gemini Office (1)
P. O. Box 516
St. Louis, Missouri 63166

Monsanto Research Corporation
Everett, Massachusetts
Attn: Dr. J. O. Smith (1)

North American Aviation Company
S&ID Division
Downey, California
Attn: Dr. James Nash (1)

Pratt & Whitney Aircraft Division
United Aircraft Corporation
East Hartford, Connecticut 06108
Attn: Librarian (1)

Radio Corporation of America
Astro Division
Heightstown, New Jersey
Attn: Dr. Seymour Winkler (1)

Radio Corporation of America
Somerville, New Jersey 08876
Attn: Dr. G. Lozier (1)

Thompson Ramo Wooldridge Inc.
23555 Euclid Avenue
Cleveland, Ohio 44117
Attn: Librarian (1)

Union Carbide Corporation
12900 Snow Road
Parma, Ohio
Attn: Dr. George E. Evans (1)

University of California
Space Science Laboratory
Berkeley, California 94704
Attn: Prof. Charles W. Tobias (1)

University of Pennsylvania
Electrochemistry Laboratory
Philadelphia, Pennsylvania 19104
Attn: Prof. John O.'M. Bockris (1)

Western Reserve University
Cleveland, Ohio
Attn: Prof. Ernest Yeager (1)

Yardney Electric Corporation
New York, New York
Attn: Dr. Paul Howard (1)

NASA, Ames Research Center
Pioneer Project
Moffett Field, California 94035
Attn: James R. Swain (1)

STATE UNIVERSITY OF NEW YORK
COLLEGE OF CERAMICS AT
ALFRED UNIVERSITY
ALFRED, N. Y.
14802

OFFICE OF RESEARCH

1 December 1965

National Aeronautics and Space Administration
Attn: Technical Reports Officer
Grants and Research Contracts
Office of Space Sciences
600 Independence Avenue
Washington, D. C. 20546

Subject: Grant NsG-384, Final Report, NASA CR-54768

1. Enclosed are copies of the Final Report for NASA Grant NsG-384.

Thomas J. Gray

Thomas J. Gray

ds
encl.

cc: per distribution list